

---

# GeoRecon: Graph-Level Representation Learning for 3D Molecules via Reconstruction-Based Pretraining

---

Shaoheng Yan<sup>1,2</sup> Zian Li<sup>1,3</sup> Muhan Zhang<sup>1,\*</sup>

<sup>1</sup>Institute for Artificial Intelligence, Peking University

<sup>2</sup>Yuanpei College, Peking University

<sup>3</sup>School of Intelligence Science and Technology, Peking University

## Abstract

The pretraining-and-finetuning paradigm has driven significant advances across domains, such as natural language processing and computer vision, with representative pretraining paradigms such as masked language modeling and next-token prediction. However, in molecular representation learning, the task design remains largely limited to node-level denoising, which is effective at modeling *local atomic environments*, yet maybe insufficient for capturing the *global molecular structure* required by graph-level property prediction tasks, such as energy estimation and molecular regression. In this work, we present GeoRecon, a novel graph-level pretraining framework that shifts the focus from individual atoms to the molecule as an integrated whole. GeoRecon introduces a graph-level reconstruction task: during pretraining, the model is trained to generate an informative graph representation capable of accurately guiding reconstruction of the molecular geometry. This encourages the model to learn coherent, global structural features rather than isolated atomic details. Without relying on additional supervision or external data, GeoRecon outperforms node-centric baselines on multiple molecular benchmarks (e.g., QM9, MD17), demonstrating the benefit of incorporating graph-level reconstruction for learning more holistic and geometry-aware molecular embeddings.

## 1 Introduction

Predicting molecular properties from three-dimensional structures is central to modern chemistry and materials science. While Density Functional Theory (Parr, 1983) delivers high-fidelity estimates, its steep computational cost prevents large-scale virtual screening. This bottleneck has driven the development of numerous deep learning approaches that aim to predict molecular properties with comparable accuracy while offering significant speed advantages (Thölke and De Fabritiis, 2022; Li et al., 2023, 2024; Gasteiger et al., 2020a, 2021; Batatia et al., 2022). Concurrently, several studies (Zaidi et al., 2023; Feng et al., 2023; Fang et al., 2022; Zhou et al., 2023; Ji et al., 2024) have adapted the pretraining-and-finetuning paradigm—originally established in computer vision (Girshick et al., 2014) and natural language processing (Radford et al., 2018)—to deep learning for molecular modeling, demonstrating effective transfer of knowledge from unlabeled molecular datasets to downstream tasks.

To date, most molecular pre-training focuses on node denoising (Zaidi et al., 2023; Feng et al., 2023) or masked atom prediction (Hou et al., 2022; Xia et al., 2023), which effectively capture local atomic interactions but *lack explicit mechanisms to encode holistic molecular geometry*. In practice, many target properties, such as energy and dipole moment (Ramakrishnan et al., 2014; Chmiela et al., 2017), are determined by *global structure* rather than local interactions. This inherent difference could lead to representation incompatibility, potentially diminishing the benefits of pre-training for global-level downstream tasks (Hu et al., 2019). To overcome these limitations, recent methods incorporate

explicit supervision via graph-level attributes (Hu et al., 2019) or frequent functional motifs (Rong et al., 2020), or adopt contrastive learning (Liu et al., 2021a). Nevertheless, these approaches are often either over specialized by hand-crafted supervisions to be broadly applicable, or are primarily designed for 2D or 2D&3D graphs, lacking inherent support for 3D molecular pre-training like denoising (Zaidi et al., 2023).

In this work, we introduce a graph-level 3D self-supervised pre-training task, which we call **Geometric Reconstruction**. Specifically, given a 3D molecule, the model is asked to *generate an informative, invariant graph-level representation*, which can be used to reconstruct the molecule’s entire 3D geometry. Since the graph-level representation is invariant to orientation, relying solely on it for reconstruction can lead to arbitrary orientations, making supervision challenging. To address this, we frame the reconstruction as a more demanding denoising task (Zaidi et al., 2023)—applying larger noise but using a lighter denoiser (decoder)—while conditioning the denoising process on the graph-level representation for guidance. This paradigm requires the model to learn a highly informative graph-level representation to compensate for the large individual noise. See Figure 1 for an illustration. Compared to directly supervising on some graph-level properties, this design is generic and task-agnostic.

To demonstrate the effectiveness of this task, we fine-tune the pre-trained model on widely adopted benchmarks, QM9 (Ramakrishnan et al., 2014) and MD17 (Chmiela et al., 2017), both of which focus on graph-level molecular property prediction. Our evaluations show that this straightforward extension generally improves the standard denoising baseline (Zaidi et al., 2023) and matches the performance of more sophisticated models that rely on external data, such as molecular spectra (Wang et al., 2025). This demonstrates that explicitly modeling graph-level structure enhances both accuracy and robustness in molecular representation learning. Additionally, we conduct several ablation studies on key design choices—such as lightweight decoder depth and noise scale in the reconstruction task—further confirming the robustness of our design.

## 2 Preliminaries

Denoising has emerged as a principled and empirically effective pretraining objective in 3D molecular representation learning (Zaidi et al., 2023; Feng et al., 2023; Zhou et al., 2023). Formally, given a slightly perturbed molecule conformation  $\tilde{\mathbf{r}} = \mathbf{r} + \boldsymbol{\epsilon} \in \mathbb{R}^{n \times 3}$  where  $n$  denotes the molecule’s node number,  $\mathbf{r} \in \mathbb{R}^{n \times 3}$  the molecule equilibrium structure and  $\boldsymbol{\epsilon}$  the Gaussian noise, the model is asked to predict the noise from the perturbed conformation  $\text{GNN}(\tilde{\mathbf{r}}) \approx \boldsymbol{\epsilon}$ . Zaidi et al. (2023) formally established the theoretical equivalence between coordinate denoising and force field prediction by leveraging the connection to score matching.

**Theorem 1** (Equivalence between denoising and force field prediction (Zaidi et al., 2023)).

$$\mathbb{E}_{q_\sigma(\tilde{\mathbf{r}}, \mathbf{r})} \left[ \left\| \text{GNN}_\theta(\tilde{\mathbf{r}}) - \nabla_{\tilde{\mathbf{r}}} \log q_\sigma(\tilde{\mathbf{r}} | \mathbf{r}) \right\|^2 \right] = \mathbb{E}_{q_\sigma(\tilde{\mathbf{r}}, \mathbf{r})} \left[ \left\| \text{GNN}_\theta(\tilde{\mathbf{r}}) - \frac{\mathbf{r} - \tilde{\mathbf{r}}}{\sigma^2} \right\|^2 \right].$$

$\mathbf{r}$  denotes the equilibrium molecular structure,  $\tilde{\mathbf{r}}$  is its perturbed version obtained by Gaussian corruption, and  $\theta$  represents the parameters of the denoising network.  $q_\sigma(\tilde{\mathbf{r}} | \mathbf{r})$  is defined as a Gaussian centered at  $\mathbf{r}$ , serving as a tractable approximation to the Boltzmann distribution  $p_{\text{physics}}(\tilde{\mathbf{r}}) \propto \exp(-E(\tilde{\mathbf{r}}))$ . Its score function corresponds to the standardized noise vector  $(\mathbf{r} - \tilde{\mathbf{r}})/\sigma^2$ . More broadly,  $p_{\text{physics}}$  can be approximated by a Gaussian mixture  $q_\sigma(\tilde{\mathbf{r}}) \sim \frac{1}{n} \sum_i \mathcal{N}(\tilde{\mathbf{r}}; \mathbf{r}_i, \sigma^2 I)$ , whose score defines a force field over noisy conformations.

This theoretical result provides a rigorous foundation for coordinate denoising as a physically grounded pretraining objective, and is empirically validated by the Coord model.

Building upon coordinate denoising, Feng et al. (2023) introduced additional dihedral angle noise  $\delta\psi \sim \mathcal{N}(0, \sigma^2 I_m)$  along rotatable bonds. For small angular displacements, these perturbations can be approximately linearized and translated into structured coordinate noise  $\boldsymbol{\epsilon}_a \sim \mathcal{N}(0, \sigma^2 \mathbf{C}\mathbf{C}^\top)$ , where  $\mathbf{C}$  denotes the transformation matrix from angular displacements to Cartesian coordinates. The resulting intermediate coordinates are given by  $\mathbf{r}_a := \mathbf{r} + \boldsymbol{\epsilon}_a$ . A second isotropic coordinate perturbation  $\boldsymbol{\epsilon}_{cd} \sim \mathcal{N}(0, \tau^2 I_{3N})$  is then added, and the model is trained to predict this final perturbation  $\boldsymbol{\epsilon}_{cd}$  during pretraining.

### 3 Method

While Feng et al. (2023) advance coordinate denoising by incorporating molecular flexibility through dihedral perturbations, their framework still focuses on node-level supervision. The model predicts local coordinate noise for each atom, but without explicit mechanisms to capture global structural context, which limits its effectiveness on graph-level tasks.

Building on the self-supervised, physically grounded coordinate-denoising objective (Zaidi et al., 2023; Feng et al., 2023), we exploit its dual benefit as both a force-field surrogate and a fine-grained geometric bias. Yet, when used in isolation, this purely node-level signal cannot enforce the global structural coherence required by graph-level property prediction.

We therefore introduce GeoRecon, a reconstruction-based pretraining framework designed to capture global molecular structure from noisy inputs. Instead of directly decoding coordinates from pooled embeddings—which often lose spatial granularity—we formulate reconstruction as a denoising process over entire molecular geometries. Specifically, we inject stronger gaussian noise into the 3D coordinates and predicting the added noise with a lightweight decoder conditioned on graph-level representations.

More precisely, GeoRecon builds upon standard coordinate denoising, but enhances its capacity to model global molecular structure by increasing the difficulty of the denoising task and providing graph-level representations as additional guidance. By injecting stronger, orientation-invariant noise into the coordinates and conditioning the decoder on a global embedding derived from clean structures, we encourage the encoder to attend to long-range dependencies and capture coherent, molecule-level geometry. This training scheme allows GeoRecon to extract more transferable representations, bridging local interactions with global structural awareness.

**Notations.** To support multi-task supervision, we construct three coordinate variants per molecule:

- `pos_clean`: the original coordinates, serving as the ground truth for the denoising task and simultaneously as the input for the reconstruction encoder task introduced in the following section, denoted by  $\mathbf{r}_i^{\text{clean}} \in \mathbb{R}^3$ , where  $i$  indexes the atom in the molecule;
- `pos_noised`: the perturbed atomic coordinates used as input for the standard denoising task, denoted by  $\mathbf{r}_i^{\text{noised}} \in \mathbb{R}^3$ ;
- `pos_rec`: a noise-scaled variant of the perturbed coordinates, used as the target in the reconstruction task; denoted by  $\mathbf{r}_i^{\text{rec}} \in \mathbb{R}^3$ .

The injected noise  $\epsilon \sim \mathcal{N}(0, \sigma^2)$  is shared across these variants. Specifically, we define:

$$\text{pos\_noised} = \text{pos\_clean} + \epsilon, \quad \text{pos\_rec} = \text{pos\_clean} + \lambda \epsilon$$

where  $\lambda \in (1, +\infty)$  modulates the reconstruction difficulty. Each target coordinate is paired with its corresponding atomic number  $z_i$  to construct the initial atomic embeddings.

Node-level embeddings are denoted as  $\{\mathbf{h}_i^{(*)}\}_{i=1}^N$ , where  $*$   $\in \{\text{denoise}, \text{rec}, \text{clean}\}$  indicates the input variant corresponding to different pretraining tasks. In contrast, the graph-level representation is denoted by  $\mathbf{g} \in \mathbb{R}^d$ , where  $d$  represents the dimensionality of the embedding space.

Pairwise edge features and edge embeddings are denoted as  $\mathbf{f}_{ij}$  and  $\mathbf{u}_{ij}^{(*)}$  respectively. For simplicity, we construct the rough edge feature  $\mathbf{d}_{ij}$  between two atoms  $i$  and  $j$  by their relative positions and define:  $\mathbf{d}_{ij} = \mathbf{r}_j^* - \mathbf{r}_i^*$ ,  $\hat{\mathbf{d}}_{ij} = \mathbf{d}_{ij} / \|\mathbf{d}_{ij}\|$ .

The model is trained to predict noise vectors  $\hat{\epsilon}_i^{(*)} \in \mathbb{R}^3$  for each atom and task, where the supervision signal is the synthetic Gaussian noise  $\epsilon_i \sim \mathcal{N}(0, \sigma^2 \mathbf{I})$  applied during pretraining.

We use  $\mathcal{L}_{\text{denoise}}$ ,  $\mathcal{L}_{\text{rec}}$ , and  $\mathcal{L}_{\text{clean}}$  to denote the three loss terms, with weighting coefficients  $\lambda_{\text{denoise}}$ ,  $\lambda_{\text{rec}}$ , and  $\lambda_{\text{clean}}$ , respectively.

#### 3.1 Model Architecture

**Shared Equivariant Encoder** At the core of GeoRecon is an 8-layer SE(3)-equivariant transformer encoder adapted from TorchMD-Net (Thölke and De Fabritiis, 2022). The encoder operates on molecular graphs defined by atomic numbers  $\{z_i\}$  and spatial coordinates  $\{\mathbf{r}_i^*\}$ .

Each node is initialized via a learnable embedding of its atomic type, optionally enriched through distance-aware neighbor aggregation. Edge features are computed by applying radial basis function (RBF) expansion to interatomic distances, modulated by a smooth cosine cutoff, while directional geometry is encoded by the normalized displacement vector:

$$\mathbf{f}_{ij} = \text{RBF}(\|\mathbf{d}_{ij}\|) \cdot \text{CUTOFF}(\|\mathbf{d}_{ij}\|).$$

At each layer, scalar and vector-valued features are jointly updated via attention-weighted message passing over neighboring nodes, incorporating edge attributes and directional information. The entire layer can be compactly written as:

$$(\mathbf{h}_i^{(l+1)}, \mathbf{u}_i^{(l+1)}) = \text{EQUIATTN}^{(l)} \left( \mathbf{h}_i^{(l)}, \mathbf{u}_i^{(l)}, \{\mathbf{h}_j^{(l)}, \mathbf{f}_{ij}, \hat{\mathbf{d}}_{ij}\}_{j \in \mathcal{N}(i)} \right),$$

where  $\mathbf{h}_i^{(l)} \in \mathbb{R}^d$  and  $\mathbf{u}_i^{(l)} \in \mathbb{R}^{3 \times d}$  denote the scalar and vector representations, respectively. For simplicity, we omit the task-specific superscript (\*) in the notations, as all tasks are treated in the same way. Residual connections and layer normalization are applied at each layer.

**Denoising Head** The denoising head is designed to reverse the synthetic perturbation applied during pretraining. Specifically, random Gaussian noise  $\epsilon$  is added to the 3D coordinates of each atom at the data processing stage. The model is trained to predict this noise vector at each node with a mean squared error (MSE) loss:

$$\hat{\epsilon}_i = \text{MLP}_{\text{denoise}}(\mathbf{h}_i)$$

$$\mathcal{L}_{\text{denoise}} = \frac{1}{N} \sum_i \|\hat{\epsilon}_i - \epsilon_i\|_2^2 \sim \frac{\sigma^2}{k_B T} \mathbf{F}$$

According to Equation (1), the equivalence between coordinate denoising and force field learning under the Boltzmann distribution assumption can be readily established. A brief derivation is included in the appendix A for completeness and reference.

For clarity, the symbol  $\sim$  above denotes that the denoising objective form is approximately equivalent to learning the molecular force field, up to a constant factor. That is, minimizing the MSE between predicted and true noise vectors corresponds to estimating the gradient of the potential energy surface, which governs atomic forces in physical systems. This interpretation is also supported by the general connection between denoising and score matching established in Vincent (2011).

To fully leverage the clean molecular conformations already processed during pretraining, we integrate them into the denoising pipeline as well. Specifically, clean molecules—with zero perturbation—are passed through the same encoder and denoising head. Their supervision target is a zero noise vector  $\epsilon_i = \mathbf{0}$ , naturally enforcing representational consistency between clean and noised structures. This unifies the treatment of clean and noised molecules under a single objective, regularizing the encoder without requiring additional components or losses. The denoising loss on clean structures is denoted by  $\mathcal{L}_{\text{clean}}$ . To evaluate the impact of the auxiliary clean alignment task, we conduct additional ablation studies in Appendix C.

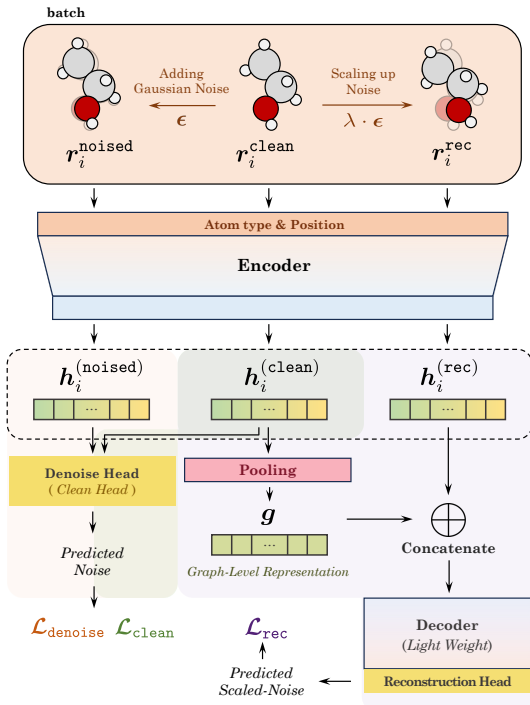


Figure 1: Overview of the GeoRecon framework. Given a molecular structure with atom types and 3D coordinates, the model encodes it using eight layers of SE(3)-equivariant attention. A pooled graph-level representation is fused with node embeddings and passed to a lightweight decoder to predict scaled noise. Additional denoising and clean heads regularize local features during pretraining. The pretrained encoder is then finetuned for downstream molecular property prediction tasks.

**Reconstruction Head with Graph-Level Conditioning** The reconstruction head in GeoRecon is designed to predict the coordinate noise applied to heavily perturbed molecular inputs, rather than directly reconstructing the original coordinates. It leverages global semantic information  $\mathbf{g}$  distilled from clean conformations to guide this denoising process. Unlike standard autoencoders that decode absolute positions, our approach treats reconstruction as a tougher denoising task—applying stronger noise to the input and predicting the corresponding perturbation under the guidance of a lightweight decoder conditioned on the graph-level embedding. This formulation not only avoids ambiguity due to global orientation, but also promotes the learning of structure-aware representations aligned with whole-molecule geometry.

To construct the conditioning signal, the clean input undergoes a complete forward pass through the encoder, producing node-level representations  $\{\mathbf{h}_i^{(\text{clean})}\}$ . These are aggregated via mean pooling to yield a graph-level vector:

$$\mathbf{g} := \text{AGGR} \left( \bigoplus_{i=1}^N \mathbf{h}_i^{(\text{clean})} \right) = \frac{1}{N} \sum_{i=1}^N \mathbf{h}_i^{(\text{clean})}.$$

The resulting vector  $\mathbf{g}$  encapsulates holistic structural semantics and is broadcasted to all nodes in the reconstruction input. We adopt mean pooling for its simplicity and stability under coordinate perturbations, though more sophisticated pooling strategies are compatible with our framework. Each node concatenates this global vector with its local features  $\mathbf{h}_i^{(\text{rec})}$ , forming the input to a lightweight decoder:

$$\mathbf{z}_i = \text{CONCAT}(\mathbf{g}, \mathbf{h}_i^{(\text{rec})}), \quad \hat{\epsilon}_i^{(\text{rec})} = \text{MLP}_{\text{rec}}(\mathbf{z}_i), \quad \mathcal{L}_{\text{rec}} = \frac{1}{N} \sum_i^N \|\hat{\epsilon}_i^{(\text{rec})} - \lambda \cdot \epsilon_i\|_2^2.$$

Here,  $\lambda$  is the fixed scaling factor that determines the difficulty of the reconstruction task, as introduced above. By increasing the noise level in the reconstruction targets  $r_i^{\text{rec}}$ , the model is encouraged to place greater emphasis on global context during decoding. This design implicitly guides the encoder to embed longer-range geometric dependencies into the graph-level representation  $\mathbf{g}$ , enhancing its ability to capture coherent molecular structures beyond local neighborhoods.

As a result, the learned latent space becomes both locally descriptive—sensitive to fine-grained atomic perturbations—and globally coherent, reflecting the overall molecular topology. This dual expressiveness contributes to improved generalization in downstream molecular property prediction tasks, particularly those sensitive to spatial organization, such as total energy, dipole moment, and orbital energy estimation.

### 3.2 Multi-Task Training Objective

To jointly optimize local and global aspects of molecular geometry, we combine the three pretraining objectives into a unified loss:

$$\mathcal{L}_{\text{total}} = \lambda_{\text{denoise}} \mathcal{L}_{\text{denoise}} + \lambda_{\text{rec}} \mathcal{L}_{\text{rec}} + \lambda_{\text{clean}} \mathcal{L}_{\text{clean}}.$$

Each component provides complementary supervision: the denoising loss captures local geometric regularities, the reconstruction loss promotes global structural awareness, and the clean alignment term is introduced to reuse the clean conformations during pretraining. Together, these tasks encourage the encoder to learn transferable representations that are effective across both node-level and graph-level downstream objectives. The loss weights are empirically chosen to ensure that the magnitudes of individual loss terms are balanced during training.

## 4 Experiments

### 4.1 Basic Setup

**Training Settings.** We pretrain GeoRecon on a large-scale 3D molecular datasets PCQM4Mv2 (Hu et al., 2021). Pretraining uses the Adam optimizer with a learning rate of  $4 \times 10^{-4}$  and cosine decay scheduling over 400k steps, with a batch size of 50. The encoder consists of 8 SE(3)-equivariant attention layers with 256-dimensional embeddings and 8 attention heads. During pretraining, Gaussian

noise with a standard deviation of  $0.04 \text{ \AA}$  is added to atomic coordinates. During finetuning, all tasks share the same pretrained encoder, followed by task-specific heads and loss functions adapted to the target property type. We adopt a full fine-tuning protocol where all model parameters are updated during downstream training.

All main experiments were conducted on NVIDIA RTX 4090 GPUs. Specifically, pretraining was performed using  $4 \times$  RTX 4090 GPUs (24GB each) over 400k steps, while downstream fine-tuning on each task was carried out using a single RTX 4090 GPU.

**Baselines.** Our method is built upon the denoising task, with an additional reconstruction auxiliary task. Therefore, *our primary direct comparison is with the denoising baseline Coord* (Zaidi et al., 2023). To clearly highlight improvements over this baseline, we mark them in **green** in Tables 1 and 2. Furthermore, we include comparisons to traditional methods without pre-training to demonstrate the benefits of pretraining, as well as to several pre-training approaches:

- **Training from scratch:** SchNet (Schütt et al., 2018) employs continuous-filter convolutions to model quantum interactions in molecules. EGNN (Satorras et al., 2021) introduces equivariant message passing under Euclidean transformations. DimeNet (Gasteiger et al., 2020b) incorporate directional information via angular message passing. DimeNet++ (Gasteiger et al., 2020a) is an enhanced version of DimeNet, offering improved efficiency and accuracy. PaiNN (Schütt et al., 2021) utilizes equivariant message passing tailored for predicting tensorial properties and molecular spectra. SphereNet (Liu et al., 2021b) enhances spatial reasoning using spherical coordinates. TorchMD-Net (Thölke and De Fabritiis, 2022) applies equivariant transformers to molecular dynamics tasks.
- **Pretraining then finetune:** Transformer-M (Luo et al., 2022) is a versatile model capable of processing both 2D and 3D molecular data through separate encoding channels. SE(3)-DDM (Liu et al., 2022) pretrains via denoising distance matching under SE(3)-invariance. 3D-EMGPJiao et al. (2023) leverages energy-motivated objectives for equivariant pretraining. Coord (Zaidi et al., 2023) applies coordinate denoising for geometry-aware representation learning. MolSpectra (Wang et al., 2025) introduces spectral prediction as an auxiliary task, enriching molecular representations with quantum-informed supervision.

Although MolSpectra also builds upon Coord codebase, it incorporates auxiliary spectral information derived from analytical force fields during pretraining. This reliance on external physical supervision makes it methodologically distinct from our purely geometry-driven and task-agnostic framework, and thus not suitable as a core baseline for our evaluation.

## 4.2 QM9: Prediction of Various Molecular Properties

We first evaluate our method on QM9 dataset. QM9 (Ramakrishnan et al., 2014) is a widely-used benchmark for quantum machine learning on small organic molecules, containing  $\sim 134\text{k}$  samples composed of H, C, N, O, F atoms. Each sample provides an equilibrium 3D geometry along with 12 quantum chemical properties computed via DFT. These include dipole moment ( $\mu$ ), isotropic polarizability ( $\alpha$ ), frontier orbital energies (HOMO, LUMO, and their gap), enthalpies ( $U, U_0, H, G$ ), zero-point vibrational energy (ZPVE), electronic spatial extent ( $R^2$ ), and heat capacity at 298.15K ( $C_v$ ), all treated as regression targets. We follow the standard data split with 110k molecules for training, 10k for validation, and the remaining for testing. Mean Absolute Error (MAE) is used as the evaluation metric. For each target property, we attach a scalar regression head to the pretrained encoder and fine-tune the entire model.

See Table 1 for results. As shown, GeoRecon achieves strong performance across a range of molecular property prediction tasks. GeoRecon achieves the best performance across all baselines on the  $U, U_0$ , and  $H$  tasks. Compared to our backbone Coord, GeoRecon shows *noticeable improvements* on key targets including  $\mu, \alpha$ , HOMO, LUMO, and gap. Interestingly, it also outperforms MolSpectra, the best performing baseline, on ZPVE  $R^2$ , *despite not relying on external spectral data*. These results support the effectiveness of incorporating graph-level reconstruction in pretraining and demonstrate that our method enhances the encoder’s ability to capture both fine-grained and global molecular structure.

Table 1: MAE ( $\downarrow$ ) on QM9 property prediction. Best and second-best results are **bolded** and underlined, respectively. Aver-rank is the mean of per-metric ranks. The methods are divided into two groups: training from scratch and pre-training then fine-tuning. Green text indicates the relative improvement (%) over the base model; red indicates degradation. During pretraining, the loss weights  $\lambda_{\text{denoise}}$ ,  $\lambda_{\text{rec}}$ , and  $\lambda_{\text{clean}}$  were set to 1, 0.5, and 10, respectively.

	$\mu$ (D)	$\alpha$ ( $a_0^3$ )	homo (meV)	lumo (meV)	gap (meV)	$R^2$ ( $a_0^3$ )	ZPVE (meV)	$U_0$ (meV)	$U$ (meV)	$H$ (meV)	$G$ (meV)	$C_p$ ( $\frac{\text{cal}}{\text{mol}\cdot\text{K}}$ )	Average rank
SchNet	0.033	0.235	41.0	34.0	63.0	0.070	1.70	14.00	19.00	14.00	14.00	0.033	10.83
EGNN	0.029	0.071	29.0	25.0	48.0	0.106	1.55	11.00	12.00	12.00	12.00	0.031	10.16
DimeNet++	0.030	<u>0.044</u>	24.6	19.5	32.6	0.330	1.21	6.32	6.28	6.53	7.56	0.023	6.33
PaiNN	0.016	0.045	27.6	20.4	45.7	<u>0.070</u>	1.28	<u>5.85</u>	<u>5.83</u>	<u>5.98</u>	7.35	0.024	5.33
SphereNet	0.025	0.045	22.8	18.9	31.1	0.270	<b>1.12</b>	6.26	6.36	6.33	7.78	0.022	5.50
TorchMD-Net	<b>0.011</b>	0.059	20.3	17.5	36.1	<b>0.033</b>	1.84	6.15	6.38	6.16	7.62	0.026	5.92
Transformer-M	0.037	<b>0.041</b>	17.5	16.2	<u>27.4</u>	0.075	<u>1.18</u>	9.37	9.41	9.39	9.63	0.022	5.92
SE(3)-DDM	0.015	0.046	23.5	19.5	40.2	0.122	1.31	6.92	6.99	7.09	7.65	0.024	7.00
3D-EMGP	0.020	0.057	21.3	18.2	37.1	0.092	1.38	8.60	8.60	8.70	9.30	0.026	7.67
MolSpectra*	<b>0.011</b>	0.048	<b>15.5</b>	<b>13.1</b>	<b>26.8</b>	0.410	1.71	<u>5.67</u>	<u>5.45</u>	<u>5.87</u>	<b>6.18</b>	<u>0.021</u>	<b>3.33</b>
Coord	0.016	0.052	17.7	14.7	31.8	0.450	1.71	6.57	6.11	6.45	6.91	<b>0.020</b>	5.67
GeoRecon (Ours)	<u>0.012</u>	0.050	<u>16.6</u>	<u>13.7</u>	30.6	0.250	1.42	<b>5.64</b>	<b>5.36</b>	<b>5.55</b>	<b>6.79</b>	0.023	<u>3.50</u>
	$\downarrow 25.00\%$	$\downarrow 3.85\%$	$\downarrow 6.21\%$	$\downarrow 6.80\%$	$\downarrow 3.77\%$	$\downarrow 44.44\%$	$\downarrow 16.96\%$	$\downarrow 14.16\%$	$\downarrow 12.27\%$	$\downarrow 13.95\%$	$\downarrow 1.74\%$	$\uparrow 15.00\%$	

\*: denotes using external data

Table 2: MAE ( $\downarrow$ ) of force prediction on MD17 dataset (kcal/mol/Å). Best and second-best results are **bolded** and underlined, respectively. Aver-rank is the mean of per-metric ranks. The methods are divided into two groups: training from scratch and pre-training then fine-tuning. Green text indicates the relative improvement (%) over the base model; red indicates degradation. During pretraining, the loss weights  $\lambda_{\text{denoise}}$ ,  $\lambda_{\text{rec}}$ , and  $\lambda_{\text{clean}}$  were set to 1, 0.5, and 10, respectively.

	Aspirin	Benzene	Ethanol	Malonaldehyde	Naphthalene	Salicylic Acid	Toluene	Uracil	Aver-rank
SphereNet	0.430	0.178	0.208	0.340	0.178	0.360	0.155	0.267	6.38
SchNet	1.350	0.310	0.390	0.660	0.580	0.850	0.570	0.560	8.75
DimeNet	0.499	0.187	0.230	0.383	0.215	0.374	0.216	0.301	7.63
PaiNN	0.338	-	0.224	0.319	0.077	0.195	0.094	0.139	-
TorchMD-Net	0.245	0.219	0.107	0.167	<u>0.059</u>	0.128	<u>0.064</u>	<u>0.089</u>	3.50
SE(3)-DDM	0.453	-	0.166	0.288	0.129	0.266	0.122	0.183	-
MolSpectra*	0.099	<u>0.097</u>	<b>0.052</b>	<b>0.077</b>	0.085	0.094	0.075	0.095	2.50
Coord	0.211	0.169	0.096	0.139	<b>0.053</b>	0.109	<b>0.058</b>	<b>0.074</b>	<u>2.25</u>
GeoRecon (Ours)	<b>0.068</b>	<b>0.048</b>	<u>0.057</u>	<u>0.093</u>	0.073	<b>0.069</b>	0.068	0.098	<b>2.13</b>
	$\downarrow 67.77\%$	$\downarrow 71.6\%$	$\downarrow 40.63\%$	$\downarrow 33.09\%$	$\uparrow 37.74\%$	$\downarrow 36.7\%$	$\uparrow 17.24\%$	$\uparrow 32.43\%$	

\*: denotes using external data

### 4.3 MD17: Molecular Dynamic Prediction

We then evaluate the model on MD17 (Chmiela et al., 2017), which is a benchmark dataset for learning energy and force fields from molecular dynamics (MD) simulations. It contains ab initio molecular dynamics trajectories for small organic molecules, with atom-wise force labels and associated energy values provided for each conformation. Unlike QM9, which focuses on equilibrium properties, MD17 emphasizes modeling local geometric sensitivity under thermal perturbations, making it a challenging testbed for fine-grained prediction. We evaluate on eight commonly used molecules. For each molecule, we adopt the standard low-data regime—training on 1,000 samples, validating on 50, and testing on the remaining configurations. Following prior work, we use Mean Absolute Error (MAE) on the predicted atomic forces as the evaluation metric.

As shown in Table 2, GeoRecon demonstrates strong performance on the MD17 benchmark for force prediction. It shows *the best performance* on multiple molecules, including Aspirin (0.068), Benzene (0.048), and Salicylic Acid (0.069), and *ranks among the top three* on others such as Ethanol and Malonaldehyde. While not consistently the best across all targets, our method performs competitively against both pretraining-based and fully supervised baselines. These results support the effectiveness of incorporating graph-level reconstruction in modeling fine-grained molecular dynamics, and suggest that integrating global structural information can enhance local force prediction accuracy without additional overhead.

## 4.4 Ablation Study

To assess the contributions of different hyperparameters in our GeoRecon framework, we conduct ablation studies along three axes: decoder depth  $L$ , reconstruction noise scale  $\lambda$ , and reconstruction loss weight  $\lambda_{\text{rec}}$ .

**Effect of Decoder Depth and Noise Scale.** We vary the number of layers  $L \in \{3, 4, 5\}$  in the lightweight decoder and the reconstruction noise scale  $\lambda \in \{1.0, 1.5\}$ , which controls the magnitude of perturbation in the reconstruction targets.

The experiments results are shown in Table 3. These results suggest an interaction between decoder depth and noise scale. When the lightweight decoder is shallow (e.g.,  $L = 3$  or  $L = 4$ ), increasing the noise scale from  $\lambda = 1.0$  to  $\lambda = 1.5$  improves downstream performance, likely because stronger perturbations force the encoder to rely more heavily on the global representation to support accurate reconstruction.

However, when the decoder becomes deeper ( $L = 5$ ), it gains sufficient capacity to locally denoise without depending as much on the global context. As a result, increasing the noise scale may not bring further benefit, and can even lead to performance degradation due to a mismatch between input difficulty and the model’s reliance on global structure. The results suggest that shallower decoders rely more on graph-level guidance, supporting our core hypothesis about the need for global conditioning.

**Effect of Reconstruction Loss Weight.** In our ablation study with 30-epoch pretraining and a CosineWarmup schedule, we varied the reconstruction loss weight  $\lambda_{\text{rec}} \in \{0.40, 0.45, 0.50\}$  while fixing decoder depth  $L = 5$  and noise scale  $\lambda = 1.0$ .

The results in Table 5 reveal a non-monotonic trend as  $\lambda_{\text{rec}}$  varies. A low weight (0.40) leads to better performance on HOMO, while higher values (e.g., 0.50) improve LUMO and gap. The intermediate setting ( $\lambda_{\text{rec}} = 0.45$ ) achieves the most balanced performance. The results suggest that  $\lambda_{\text{rec}}$  modulates the encoder’s representational focus. We interpret this as an empirical observation that stronger reconstruction constraints may influence the encoder’s global focus, motivating further analysis.

## 5 Related Work

**Geometric Graph Neural Networks** Early methods incorporated 3D geometry into GNNs via continuous-filter convolutions and directional message passing. SchNet (Schütt et al., 2018) operates directly on Cartesian coordinates to predict energy and forces. DimeNet (Gasteiger et al., 2020b) and DimeNet++ (Gasteiger et al., 2020a) capture angular information, improving performance and efficiency. GemNet (Gasteiger et al., 2021) further enhances accuracy using multi-hop and higher-order geometric features. Meanwhile, EGNN (Satorras et al., 2021) and SE(3)-Transformer (Fuchs et al., 2020) encode Euclidean symmetries through equivariance, matching tensor-based models with lower complexity.

**Self-Supervised Denoising Pretraining** Self-supervised denoising has emerged as a principled means to leverage unlabeled molecular conformations. Coord pretraining (Zaidi et al., 2023) demonstrates that training a GNN to remove Gaussian perturbations from equilibrium structures is mathemat-

Table 3: Effect of decoder depth  $L$  and noise scale  $\lambda$  on finetuning performance (MAE↓). Each group reports HOMO, LUMO, and GAP errors, the best result in each task is highlighted in **bold**, and the second-best is underlined, respectively. (Pre-training 10 epoch)

$\lambda$	Task	$L = 3$	$L = 4$	$L = 5$
1.0	HOMO	0.01812	0.02028	<u>0.01687</u>
	LUMO	0.01506	0.02110	<b>0.01368</b>
	GAP	<b>0.03132</b>	0.04220	<u>0.03157</u>
1.5	HOMO	0.01722	<b>0.01661</b>	0.01688
	LUMO	<u>0.01472</u>	0.01451	0.01497
	GAP	0.03218	0.03307	0.03238

Table 4: Effect of reconstruction loss weight  $\lambda_{\text{rec}}$  with fixed  $L = 5$ ,  $\lambda = 1$ , the best result in each task is highlighted in **bold**. (Pre-training 30 epoch)

$\lambda_{\text{rec}}$	HOMO	LUMO	GAP
0.4	<b>0.01630</b>	0.01509	0.03345
0.45	0.01756	<b>0.01379</b>	<b>0.03141</b>
0.5	0.01659	0.01403	0.03227

ically equivalent to learning the underlying molecular force field, markedly improving downstream QM9 performance under limited labels. Frad (Feng et al., 2023) furthers this concept by jointly perturbing dihedral angles and Cartesian coordinates, better emulating realistic conformational variations. SliDe (Ni et al., 2024) augments denoising tasks with classical force-field priors (bond lengths, angles, torsions), grounding the learned representation in established physical interactions. More recently, MolSpectra (Wang et al., 2025) integrates multimodal energy-level spectra via contrastive reconstruction, enriching the model’s access to discrete quantum information without external labels.

**Multi-Task and Multi-Fidelity Learning** Multi-task learning leverages shared structure across quantum properties or fidelity levels to improve sample efficiency and generalization. Predicting multiple QM9 targets jointly promotes embedding reuse and reduces overfitting. In the multi-fidelity setting, Ren et al. (2023) combine expensive CC labels with cheaper DFT data to achieve CC-level accuracy using far fewer CC samples. These approaches help mitigate data scarcity while balancing accuracy and cost.

**Graph-Level Pretraining in Molecular Representation Learning** While early GNN pretraining efforts focused on node-level tasks such as masked atom prediction (Hu et al., 2019; Hou et al., 2022; Xia et al., 2023), recent work has increasingly explored graph-level objectives to capture molecule-wide structural signals. For instance, GROVER (Rong et al., 2020) introduces motif prediction as a graph-level auxiliary task, encouraging the model to identify recurring functional substructures across molecules. MGSSL (Zhang et al., 2021) further extends this idea by generating molecular graphs motif-by-motif, injecting global inductive biases into the pretraining phase. GraphCL (You et al., 2020) and GCC (Qiu et al., 2020) apply graph-level contrastive learning via augmented graph views, promoting representation consistency at the whole-graph level.

Other approaches have leveraged cross-modal or multi-scale alignment to improve global structure modeling. GraphMVP (Liu et al., 2021a), for example, aligns 2D molecular graphs with their corresponding 3D conformers, transferring geometric awareness into 2D encoders through contrastive learning. Uni-Mol2 (Ji et al., 2024) introduces a two-track transformer architecture that jointly encodes atomic, graph-level, and spatial features during pretraining. While effective, many of these methods require additional modalities, large-scale augmentation pipelines, or complex model designs. In contrast, our method employs a single graph-level reconstruction objective—conditioned on pooled global embeddings—built directly atop coordinate denoising, achieving strong downstream performance without auxiliary data or significant overhead.

## 6 Conclusion, Limitations and Future Work

We introduced **GeoRecon**, a reconstruction-based pretraining framework that captures both local interactions and global molecular structures in 3D molecular graphs. By conditioning denoising on graph-level representations derived from clean conformations, GeoRecon effectively learns geometry-aware embeddings that are well-suited for downstream tasks. Despite not achieving the best results on every target, GeoRecon significantly improves upon the base model and narrows the gap to SOTA across diverse properties. These results highlight the complementary role of graph-level reconstruction in enhancing node-level pretraining, offering a conceptually simple yet effective design that can be integrated into a wide range of molecular learning frameworks. Furthermore, GeoRecon’s physically grounded and modular structure makes it compatible with various 3D molecular backbones.

**Limitations.** While GeoRecon demonstrates strong performance, several limitations remain. Our evaluation is currently limited to standard equilibrium datasets (QM9 and MD17), leaving open the question of generalization to more diverse, larger-scale, or noisy molecular systems, such as biomolecules or experimental crystal structures.

**Future Work.** Future directions include scaling GeoRecon to these more complex domains, integrating flexible attention-based backbones, and exploring contrastive or generative formulations of graph-level supervision. Moreover, while many graph-level pretraining methods—such as GROVER and GraphMAE—have shown strong results on biochemical property datasets (e.g., ESOL, Lipo, Malaria, CEP, Davis, and KIBA), they have not been evaluated on quantum-chemical benchmarks like QM9 or MD17. Extending our evaluation to include these biochemical datasets would enable a more holistic and cross-domain comparison of graph-level molecular pretraining strategies.

## References

- Ilyes Batatia, David P Kovacs, Gregor Simm, Christoph Ortner, and Gábor Csányi. Mace: Higher order equivariant message passing neural networks for fast and accurate force fields. *Advances in neural information processing systems*, 35:11423–11436, 2022.
- Stefan Chmiela, Alexandre Tkatchenko, Huziel E Sauceda, Igor Poltavsky, Kristof T Schütt, and Klaus-Robert Müller. Machine learning of accurate energy-conserving molecular force fields. *Science Advances*, 3(5):e1603015, 2017.
- Xiaomin Fang, Lihang Liu, Jieqiong Lei, Donglong He, Shanzhuo Zhang, Jingbo Zhou, Fan Wang, Hua Wu, and Haifeng Wang. Geometry-enhanced molecular representation learning for property prediction. *Nature Machine Intelligence*, 4(2):127–134, 2022.
- Shikun Feng, Yuyan Ni, Yanyan Lan, Zhi-Ming Ma, and Wei-Ying Ma. Fractional denoising for 3d molecular pre-training. In *International Conference on Machine Learning (ICML)*, 2023.
- Fabian B Fuchs, Daniel E Worrall, Volker Fischer, and Max Welling. Se(3)-transformers: 3d rotation equivariant attention networks. In *Advances in Neural Information Processing Systems 33 (NeurIPS)*, 2020.
- Johannes Gasteiger, Shankari Giri, Johannes T Margraf, and Stephan Günnemann. Fast and uncertainty-aware directional message passing for non-equilibrium molecules. *arXiv preprint arXiv:2011.14115*, 2020a.
- Johannes Gasteiger, Janek Groß, and Stephan Günnemann. Directional message passing for molecular graphs. *arXiv preprint arXiv:2003.03123*, 2020b.
- Johannes Gasteiger, Florian Becker, and Stephan Günnemann. Gemnet: Universal directional graph neural networks for molecules. *Advances in Neural Information Processing Systems*, 34: 6790–6802, 2021.
- Ross Girshick, Jeff Donahue, Trevor Darrell, and Jitendra Malik. Rich feature hierarchies for accurate object detection and semantic segmentation. In *Proceedings of the IEEE Conference on Computer Vision and Pattern Recognition (CVPR)*, June 2014.
- Zhenyu Hou, Xiao Liu, Yukuo Cen, Yuxiao Dong, Hongxia Yang, Chunjie Wang, and Jie Tang. Graphmae: Self-supervised masked graph autoencoders. In *Proceedings of the 28th ACM SIGKDD conference on knowledge discovery and data mining*, pages 594–604, 2022.
- Weihua Hu, Bowen Liu, Joseph Gomes, Marinka Zitnik, Percy Liang, Vijay Pande, and Jure Leskovec. Strategies for pre-training graph neural networks. *arXiv preprint arXiv:1905.12265*, 2019.
- Weihua Hu, Matthias Fey, Hongyu Ren, Maho Nakata, Yuxiao Dong, and Jure Leskovec. Ogb-lsc: A large-scale challenge for machine learning on graphs. *arXiv preprint arXiv:2103.09430*, 2021.
- Xiaohong Ji, Zhen Wang, Zhifeng Gao, Hang Zheng, Linfeng Zhang, Guolin Ke, et al. Uni-mol2: Exploring molecular pretraining model at scale. *arXiv preprint arXiv:2406.14969*, 2024.
- Rui Jiao, Jiaqi Han, Wenbing Huang, Yu Rong, and Yang Liu. Energy-motivated equivariant pre-training for 3d molecular graphs. In *Proceedings of the AAAI Conference on Artificial Intelligence*, volume 37, pages 8096–8104, 2023.
- Zian Li, Xiyuan Wang, Yinan Huang, and Muhan Zhang. Is distance matrix enough for geometric deep learning? *Advances in Neural Information Processing Systems*, 36:37413–37447, 2023.
- Zian Li, Xiyuan Wang, Shijia Kang, and Muhan Zhang. On the completeness of invariant geometric deep learning models. *arXiv preprint arXiv:2402.04836*, 2024.
- Shengchao Liu, Hanchen Wang, Weiyang Liu, Joan Lasenby, Hongyu Guo, and Jian Tang. Pre-training molecular graph representation with 3d geometry. *arXiv preprint arXiv:2110.07728*, 2021a.
- Shengchao Liu, Hongyu Guo, and Jian Tang. Molecular geometry pretraining with se (3)-invariant denoising distance matching. *arXiv preprint arXiv:2206.13602*, 2022.

- Shitong Liu, Xuyang Wang, Weiyang Liu, Li Wang, Cheng Ju, and Jian Tang. Spherical message passing for 3d graph networks. *arXiv preprint arXiv:2102.05013*, 2021b.
- Shengjie Luo, Tianlang Chen, Yixian Xu, Shuxin Zheng, Tie-Yan Liu, Liwei Wang, and Di He. One transformer can understand both 2d & 3d molecular data. *arXiv preprint arXiv:2210.01765*, 2022.
- Yuyan Ni, Shikun Feng, Wei-Ying Ma, Zhi-Ming Ma, and Yanyan Lan. Sliced denoising: A physics-informed molecular pre-training method. In *International Conference on Learning Representations (ICLR)*, 2024.
- R G Parr. Density functional theory. *Annual Review of Physical Chemistry*, 34(Volume 34, 1983):631–656, 1983. ISSN 1545-1593. doi: <https://doi.org/10.1146/annurev.pc.34.100183.003215>. URL <https://www.annualreviews.org/content/journals/10.1146/annurev.pc.34.100183.003215>.
- Jiezhong Qiu, Qibin Chen, Yuxiao Dong, Jing Zhang, Hongxia Yang, Ming Ding, Kuansan Wang, and Jie Tang. Gcc: Graph contrastive coding for graph neural network pre-training. In *Proceedings of the 26th ACM SIGKDD international conference on knowledge discovery & data mining*, pages 1150–1160, 2020.
- Alec Radford, Karthik Narasimhan, Tim Salimans, Ilya Sutskever, et al. Improving language understanding by generative pre-training. 2018.
- Raghuathan Ramakrishnan, Pavlo O Dral, Matthias Rupp, and O Anatole von Lilienfeld. Quantum chemistry structures and properties of 134 kilo molecules. *Scientific data*, 1(1):1–7, 2014.
- Gao-Peng Ren, Yi-Jian Yin, Ke-Jun Wu, and Yuchen He. Force field-inspired molecular representation learning for property prediction. *Journal of Cheminformatics*, 15(1):17, 2023. doi: 10.1186/s13321-023-00691-2.
- Yu Rong, Yatao Bian, Tingyang Xu, Weiyang Xie, Ying Wei, Wenbing Huang, and Junzhou Huang. Self-supervised graph transformer on large-scale molecular data. *Advances in neural information processing systems*, 33:12559–12571, 2020.
- Victor Garcia Satorras, Emiel Hoogeboom, and Max Welling. E(n) equivariant graph neural networks. In *International Conference on Machine Learning (ICML)*, pages 9323–9332, 2021.
- Kristof Schütt, Oliver Unke, and Michael Gastegger. Equivariant message passing for the prediction of tensorial properties and molecular spectra. In *International Conference on Machine Learning*, pages 9377–9388. PMLR, 2021.
- Kristof T Schütt, Huziel E Sauceda, P-J Kindermans, Alexandre Tkatchenko, and K-R Müller. SchNet—a deep learning architecture for molecules and materials. *The Journal of Chemical Physics*, 148(24), 2018.
- Peter Thölke and Gianni De Fabritiis. Torchmd-net: Equivariant transformers for neural network based molecular potentials. *arXiv preprint arXiv:2202.02541*, 2022.
- Pascal Vincent. A connection between score matching and denoising autoencoders. *Neural computation*, 23(7):1661–1674, 2011.
- Liang Wang, Shaozhen Liu, Yu Rong, Deli Zhao, Qiang Liu, Shu Wu, and Liang Wang. MolSpectra: Pre-training 3d molecular representation with multi-modal energy spectra. *arXiv preprint arXiv:2502.16284*, 2025.
- Jun Xia, Chengshuai Zhao, Bozhen Hu, Zhangyang Gao, Cheng Tan, Yue Liu, Siyuan Li, and Stan Z Li. Mole-bert: Rethinking pre-training graph neural networks for molecules. 2023.
- Yuning You, Tianlong Chen, Yongduo Sui, Ting Chen, Zhangyang Wang, and Yang Shen. Graph contrastive learning with augmentations. *Advances in neural information processing systems*, 33: 5812–5823, 2020.

Sheheryar Zaidi, Michael Schaarschmidt, James Martens, Hyunjik Kim, Yee Whye Teh, Alvaro Sanchez-Gonzalez, Peter W Battaglia, Razvan Pascanu, and Jonathan Godwin. Pre-training via denoising for molecular property prediction. In *International Conference on Learning Representations (ICLR)*, 2023.

Zaixi Zhang, Qi Liu, Hao Wang, Chengqiang Lu, and Chee-Kong Lee. Motif-based graph self-supervised learning for molecular property prediction. *Advances in Neural Information Processing Systems*, 34:15870–15882, 2021.

Gengmo Zhou, Zhifeng Gao, Qiankun Ding, Hang Zheng, Hongteng Xu, Zhewei Wei, Linfeng Zhang, and Guolin Ke. Uni-mol: A universal 3d molecular representation learning framework. 2023.

## A Proof of equivariance between denoise and force field learning

We briefly revisit the theoretical grounding of denoising as an approximation to physical force learning, as established by prior work (Zaidi et al., 2023).

Let  $\mathbf{x}_{i(j)}$  denote the position of atom  $i$  in molecule  $j$ , where each conformation  $\mathbf{x}_i \in \mathbb{R}^{3N}$  is mean-centered to ensure  $\sum_j \mathbf{x}_{i(j)} = \mathbf{0}$ , thereby lying in a  $(3N - 3)$ -dimensional subspace. Denote the potential energy function as  $U(\mathbf{x})$ , which maps geometric configurations to their corresponding energy levels. The negative gradient  $-\nabla_{\mathbf{x}}U(\mathbf{x})$  corresponds to the force field and serves as the prediction target in force-learning tasks. The distribution of molecular conformations  $\mathbf{x}$  is denoted as  $p_{\text{phy}}(\mathbf{x})$ , which follows the Boltzmann distribution and takes the form  $A \exp(-U(\mathbf{x})/kT)$  where  $A$  is a normalization constant,  $k$  is the Boltzmann constant, and  $T$  is the temperature.

From a probabilistic perspective, the distribution of the noised coordinates  $\mathbf{x}^{\text{denoise}}$  can be expressed as a marginalization over the clean coordinates:

$$p(\mathbf{x}^{\text{denoise}}) = \int p_{\tau}(\mathbf{x}^{\text{denoise}}|\mathbf{x}^{\text{clean}})p(\mathbf{x}^{\text{clean}})d\mathbf{x}^{\text{clean}}$$

Here, the conditional distribution  $p_{\tau}(\mathbf{x}^{\text{denoise}}|\mathbf{x}^{\text{clean}})$  is modeled as a Gaussian in the  $(3N - 3)$ -dimensional mean-centered subspace, with isotropic variance  $\tau^2$ . According to Vincent (2011), Denoising Score Match (DSM) is equivalent to Explicit Score Matching (ESM):

$$\begin{aligned}\mathcal{L}_{\text{DSM}} &= \mathbb{E}_{p_{\tau}(\mathbf{x}^{\text{denoise}}, \mathbf{x}^{\text{clean}})} \left\| \text{GNN}_{\theta}(\mathbf{x}^{\text{denoise}}) - \frac{\partial \log p_{\tau}}{\partial \mathbf{x}^{\text{denoise}}} \right\|^2 \\ &= \mathbb{E}_{p_{\tau}(\mathbf{x}^{\text{denoise}}, \mathbf{x}^{\text{clean}})} \left\| \text{GNN}_{\theta}(\mathbf{x}^{\text{denoise}}) - \frac{1}{\tau^2}(\mathbf{x}^{\text{denoise}} - \mathbf{x}^{\text{clean}}) \right\|^2 \\ &= \mathbb{E}_{p_{\text{phy}}(\mathbf{x}^{\text{denoise}})} \left\| \text{GNN}_{\theta}(\mathbf{x}^{\text{denoise}}) - (-\nabla U(\mathbf{x}^{\text{denoise}})) \right\|^2 + \text{Const} = \mathcal{L}_{\text{ESM}} + \text{Const}\end{aligned}$$

This establishes a theoretical bridge between denoising-based supervision and force field learning under equilibrium statistics. Accordingly, our reconstruction task, which leverages graph-level embeddings to modulate scaling denoising, is not only empirically effective but also theoretically justified through its approximation of physically meaningful gradients. This connection underlies our decision to instantiate reconstruction via a scaling denoise mechanism.

## B Supplement Ablation study

To rigorously demonstrate the contributions of our reconstruction task and the clean alignment task, we conducted an additional ablation study on them. We pretrained a RecOnly Model, which set the weight of Clean task weight into 0 and other hyperparameters keep unchanges.

The experimental results are shown in Table 5. Our method (Rec+Clean) achieves the best performance in most of the three settings, which demonstrates the effectiveness of our design. Besides, RecOnly performs better than Coord, while the lack of the Clean task leads to slight performance drop compared to Rec+Clean, suggesting that the Clean task also contributes to the overall performance.

Table 5: Effect of clean alignment (MAE↓) with fixed  $L = 5$ ,  $\lambda = 1$ , under three pre-training settings: Baseline, RecOnly, and Rec+Clean. The best result for each target is highlighted in **bold**. (Pre-training for 30 epochs)

Model	HOMO	LUMO	GAP
Coord	0.0177	0.0147	0.0318
RecOnly	<b>0.0163</b>	0.0141	0.0315
Rec+Clean	0.0166	<b>0.0137</b>	<b>0.0306</b>

## C Training parameters

Our hyperparameter settings are shown in Table 6, which closely follow those of Coord (Zaidi et al., 2023), with minimal modifications that we reduce the pretraining batch size on the QM9 dataset from 70 to 50 due to GPU memory constraints.

We have provided the codes in the supplementary materials.

Table 6: Training Configuration

	<b>Finetuning</b>		<b>Pretraining</b>	
	QM9	MD17	QM9	MD17
batch_size	128	8	50	70
cutoff_lower	0	0	0	0
cutoff_upper	5	5	5	5
ema_alpha_dy	1	1	1	1
ema_alpha_y	1	0.05	1	1
embedding_dimension	256	128	256	128
energy_weight	1	0.2	0	0
force_weight	1	0.8	1	1
inference_batch_size	128	64	70	70
lr	0.0004	0.0005	0.0004	0.0004
lr_schedule	cosine_warmup	cosine_warmup	cosine	cosine
lr_min	1e-7	1e-7	1e-7	1e-7
lr_patience	15	30	15	15
lr_warmup_steps	10000	1000	10000	10000
lr_cosine_length	100000	20000	400000	400000
max_num_neighbors	32	32	32	32
max_z	100	100	100	100
num_heads	8	8	8	8
num_layers	8	6	8	6
num_nodes	1	1	1	1
num_rbf	64	32	64	32
num_workers	6	6	6	6
precision	32	32	32	32
save_interval	10	10	1	1
test_interval	10	100	1	1
position_noise_scale	0	0.005	0.04	0.04
denoising_weight	0.1	0.1	1	1